Nonlinear Landau–Zener processes in a periodic driving field

New Journal of Physics
The open-access journal for physics

Nonlinear Landau–Zener processes in a periodic driving field

Qi Zhang[1], **Peter Hänggi**[1,2] **and Jiangbin Gong**[1,3,4]

[1] Department of Physics and Center for Computational Science and Engineering, National University of Singapore, 117542, Republic of Singapore

[2] Institut für Physik, Universität Augsburg, Universitätsstraße 1, D-86135 Augsburg, Germany

[3] NUS Graduate School for Integrative Sciences and Engineering, Singapore, 117597, Republic of Singapore

E-mail: phygj@nus.edu.sg

New Journal of Physics **10** (2008) 073008 (17pp)
Received 28 April 2008
Published 3 July 2008
Online at http://www.njp.org/
doi:10.1088/1367-2630/10/7/073008

Abstract. Effects of a periodic driving field on Landau–Zener (LZ) processes are studied using a nonlinear two-mode model that describes the mean-field dynamics of a many-body system. A variety of different dynamical phenomena in different parameter regimes of the driving field are discussed and analyzed. These include shifted, weakened, or enhanced phase dependence of nonlinear LZ (NLZ) processes, nonlinearity-enhanced population transfer in the adiabatic limit and Hamiltonian chaos on the mean-field level. The emphasis of this work is based on how the impact of a periodic driving field on LZ processes with self-interaction differs from those without self-interaction. Apart from gaining knowledge of driven NLZ processes, our findings can be used to gauge the strength of nonlinearity and for efficient manipulation of the mean-field dynamics of many-body systems.

[4] Author to whom any correspondence should be addressed.

Contents

1. Introduction

The Landau–Zener (LZ) transition [1] forms a fundamental dynamical process relevant to a variety of contexts, such as quantum control and quantum information [2]–[6], quantum dots [7], molecular clusters [8], to name a few. If the external bias involved in an LZ process is tuned adiabatically, then the LZ-tunneling probability goes to zero, yielding a robust scenario for realizing a complete quantum population inversion. If the external bias is varied non-adiabatically, then the LZ-tunneling offers a diagnostic tool for understanding the quantum dynamics. Indeed, the paramount importance of LZ processes has motivated a large body of theoretical and experimental works [9, 10].

As a very recent development, Wubs *et al* [11] studied numerically and analytically how an LZ process might be further manipulated by considering a periodic driving field. Within the rotating-wave-approximation (RWA), Wubs *et al* [11] showed that an LZ process in the presence of a driving field possesses two intriguing features. Firstly, the driving field can induce interesting quantum-interference effects between two well-separated LZ sub-processes, with the final quantum transition probability dependent upon the phase of the driving field. Secondly, contrary to a standard LZ problem, the population-inversion probability approaches zero (instead of unity) if the bias is tuned adiabatically. These findings may find novel applications of LZ processes, especially in identifying an unknown phase of a driving field or in studying decoherence timescales of a system coupled with an environment.

Generalizing LZ processes for single-quantum systems to those associated with the mean-field dynamics of interacting many-body systems, one obtains nonlinear LZ (NLZ) processes. Due to their implications for quantum control of the dynamics of Bose–Einstein condensates (BEC) [12], NLZ processes have also attracted considerable interest. Note that the meanfield dynamics of an interacting many-body system is necessarily nonlinear, and as a result simple physical intuitions based on linear LZ processes may become invalid in nonlinear cases. For example, the adiabatic following a quantum state with an external bias may break down in an NLZ process, even when the external bias varies at an infinitely slow rate [13]–[15].

Extending the work by Wubs *et al* [11] from the linear regime to the nonlinear regime, our interest here is in how a periodic driving field might affect NLZ processes. It is hoped that

a complete picture of driven NLZ processes will help make the best use of a driving field in manipulating the mean-field dynamics of many-body systems. To reach that long-term goal, it is necessary to first examine how the impact of a periodic driving field on NLZ processes differs from that on conventional LZ processes.

In our previous work [16], NLZ processes subject to a high-frequency and large-amplitude driving field were studied. There, using a high-frequency approximation, we showed that the driven NLZ dynamics can be effectively described by a stationary Hamiltonian. The spectrum of the effective Hamiltonian can have new degenerate eigenstates and hence display new topological structures that are absent in the non-driven cases. The results offer a simple approach to the complete suppression of NLZ tunneling, even when the tunneling is doomed to happen in the absence of a driving field.

This work continues to study driven NLZ dynamics, but with the parameter regimes different from those in [16]. We place our emphasis on comparisons between driven (linear) LZ processes and driven NLZ processes, thus shedding more light on the nonlinear and mean-field nature of NLZ dynamics. For example, we shall show that nonlinearity can induce significant quantum population transfer that is completely absent in linear cases. We will also show that the extent of population transfer in driven NLZ processes can be, as compared with driven LZ processes, either much more or much less sensitive to the phase of the driving field. It is hoped that our detailed results hereinafter will motivate more efforts toward better understanding and better control of many-body systems.

This paper is organized as follows. In section 2, we briefly discuss our two-mode model of NLZ processes in a periodic driving field. In section 3, we discuss the high-frequency approximation in treating NLZ processes in a high-frequency and large-amplitude driving field. In section 4, we consider a different regime of field parameters, where the RWA can be applied. In section 5, we study another parameter regime, where neither the high-frequency approximation nor the RWA is valid. Section 6 concludes this work.

2. Model of NLZ processes in an 'off-diagonal' driving field

Motivated by the model of linear driven LZ processes considered in [11], we consider a two-mode model of driven NLZ processes as follows:

$$H(t) = \frac{1}{2}\begin{pmatrix} \gamma + c(|b|^2 - |a|^2) & \Delta_C + \Delta_0 \cos(\omega t + \beta) \\ \Delta_C + \Delta_0 \cos(\omega t + \beta) & -\gamma - c(|b|^2 - |a|^2) \end{pmatrix}. \tag{1}$$

Here,

$$\gamma = \alpha t \tag{2}$$

denotes a time-dependent bias between two modes of interest and is being varied at a rate α; $|a|^2$ and $|b|^2$ represent occupation probabilities on the two modes, with the normalization condition taken as $|a|^2 + |b|^2 = 1$. The terms containing c characterize the nonlinear self-interaction of a BEC under the mean-field treatment, with the value of c proportional to the number of bosons and the s-wave scattering length [12]–[15]; Δ_C represents the static coupling between the two modes; and Δ_0 is the amplitude of an external driving, with the frequency ω and the phase parameter β. Unlike previous models for driven LZ/NLZ processes [12, 17, 18] or for coherent

destruction of tunneling [9, 19] (for a recent beautiful experimental validation of the latter phenomenon, see [20, 21]), the driving field here appears only in the off-diagonal terms of the above Hamiltonian and is hence an 'off-diagonal' driving field. That is, the external field directly modulates the coupling between the two modes, rather than modulating their energy bias. The initial state of an NLZ process is always taken as $a = 1$ and $b = 0$, and the occupation probability $|b|^2$ in the end, denoted by $|b(\infty)|^2$, is the final quantum-transition probability (or the final population transferred between the two modes). Note also that all the variables here should be understood as scaled dimensionless variables with $\hbar = 1$. Throughout, we use Δ_0 to scale. Then, $\Delta_0 = 1$, ω is in units of $\Delta_0/\hbar$, α is in units of $\Delta_0^2/\hbar$ and c is in units of Δ_0.

Within the BEC context, the above Hamiltonian may be experimentally realized in several ways. For example, one may consider a BEC in a double-well potential [22]–[25], with the barrier height periodically modulated, or by a BEC in an optical lattice occupying two bands [26], with the well-depth of the optical lattice periodically modulated. One may also regard the two modes as two internal states of a BEC, such as ^{87}Rb [27], with the energy bias γ effectively realized by the detuning of a coupling field from the resonance and the off-diagonal modulation achieved by modulating the intensity of the coupling field. Though we only refer to the BEC context hereinafter, it should be noted that this two-mode model of NLZ might be relevant to physics of Josephson junctions as well as nonlinear optics [28].

In the special case of $\Delta_0 = 0$, the above Hamiltonian reduces to the well-known model of non-driven NLZ processes [14]. Therein, the eigen-spectrum diagram as a function of γ is known to display a loop structure at the tip of the lower (upper) level for $c > \Delta_C$ ($c < -\Delta_C$). Such a loop structure, absent in linear systems, directly leads to a nonzero LZ transition probability even when γ changes adiabatically. This makes it interesting to examine what happens if an NLZ process is subject to a periodic driving field as introduced above.

Without loss of generality we will restrict ourselves to the $c > 0$ cases (cases with $c < 0$ can be mapped to those with $c > 0$). This $c > 0$ assumption requires, for example, an attractive interaction for bosons in a double-well potential or a repulsive interaction for bosons in two energy bands of an optical lattice. In current non-modulated double-well BEC experiments, typical values of $|c/\Delta_C|$ for 10^3 bosons range from $\sim 10^0$ to $\sim 10^1$ [12, 25]. For the latter two-band realization of our two-mode model, the value of c (scaled by Δ_0) can be easily tuned by controlling the maximal depth of an optical lattice potential [14].

To examine the driven NLZ dynamics (i.e. $\Delta_0 \neq 0$), we consider below three different parameter regimes. In the first high-frequency and large-amplitude regime, a high-frequency approximation can be used to obtain an effective Hamiltonian. The second regime is the RWA regime, where the driven dynamics is again understood in terms of some effective Hamiltonians. In the third regime, both the driving frequency ω and the amplitude Δ_0 are comparable to, or smaller than, the nonlinear parameter c. Our task below is to examine the driven NLZ dynamics in these three regimes.

3. High-frequency and large-amplitude driving field

The NLZ dynamics under the condition $\omega, \Delta_0 \gg \gamma_0, c, \Delta_C$ and γ_0 (where γ_0 is the initial value of γ) was first studied by us in [16] using a high-frequency approximation. For completeness and for the sake of comparison with other regimes, here we briefly revisit this regime. To that

end, we first introduce another pair of wave-function parameters (a', b')

$$\begin{aligned} a' &= \frac{a+b}{2} e^{i\frac{\Delta_0}{2\omega}\sin(\omega t+\beta)} + \frac{a-b}{2} e^{-i\frac{\Delta_0}{2\omega}\sin(\omega t+\beta)}, \\ b' &= \frac{a+b}{2} e^{i\frac{\Delta_0}{2\omega}\sin(\omega t+\beta)} - \frac{a-b}{2} e^{-i\frac{\Delta_0}{2\omega}\sin(\omega t+\beta)}. \end{aligned} \tag{3}$$

Substituting these two relations into the Hamiltonian in equation (1), one finds the equations of motion for (a', b')

$$\begin{aligned} i\frac{da'}{dt} &= \frac{1}{2}[\gamma\cdot\cos(\theta) + c\cdot\cos^2(\theta)(|b'|^2 - |a'|^2) + ic\cdot\sin(\theta)\cos(\theta)(a'^*b' - a'b'^*)]a' \\ &\quad + \frac{1}{2}[\Delta_C - i\gamma\cdot\sin(\theta) + c\cdot\sin^2(\theta)(a'^*b' - a'b'^*) + ic\cdot\sin(\theta)\cos(\theta)(|a'|^2 - |b'|^2)]b', \\ i\frac{db'}{dt} &= \frac{1}{2}[\Delta_C + i\gamma\cdot\sin(\theta) - c\cdot\sin^2(\theta)(a'^*b' - a'b'^*) - ic\cdot\sin(\theta)\cos(\theta)(|a'|^2 - |b'|^2)]a' \\ &\quad + \frac{1}{2}[-\gamma\cdot\cos(\theta) - c\cdot\cos^2(\theta)(|b'|^2 - |a'|^2) - ic\cdot\sin(\theta)\cos(\theta)(a'^*b' - a'b'^*)]b', \end{aligned} \tag{4}$$

where $\theta \equiv \frac{\Delta_0}{\omega}\sin(\omega t+\beta)$.

For sufficiently large ω, the oscillation in θ is much faster than all other timescales of the system. As such, during each period of $T = 2\pi/\omega$, the change in a' and b' is negligible and considering their averages over T will greatly reduce the equations of motion. Specifically, upon a time averaging the odd functions of t in equation (4) vanish and the effective equations of motion become

$$\begin{aligned} i\frac{da'}{dt} &= \frac{1}{2}[\gamma' + c_Z(|b'|^2 - |a'|^2)]a' + \frac{1}{2}[\Delta_C + c_Y(a'^*b' - a'b'^*)]b' \\ i\frac{db'}{dt} &= \frac{1}{2}[\Delta_C - c_Y(a'^*b' - a'b'^*)]a' + \frac{1}{2}[-\gamma' - c_Z(|b'|^2 - |a'|^2)]b', \end{aligned} \tag{5}$$

where $\gamma' = \gamma\langle\cos(\theta)\rangle_T = \gamma J_0(\Delta_0/\omega)$, $c_Z = c\langle\cos^2(\theta)\rangle_T = c[1 + J_0(2\Delta_0/\omega)]/2$, $c_Y = c\langle\sin^2(\theta)\rangle_T = c[1 - J_0(2\Delta_0/\omega)]/2$ and J_0 is the zeroth-order Bessel function of the first kind. Apparently, these newly defined parameters reflect the action of the high-frequency driving field.

Based on equation (5), we can define the following effective Hamiltonian:

$$H_{\text{eff}} = \frac{1}{2}\begin{pmatrix} \gamma + c_Z(|b|^2 - |a|^2) & \Delta_C + c_Y(a^*b - ab^*) \\ \Delta_C - c_Y(a^*b - ab^*) & -\gamma - c_Z(|b|^2 - |a|^2) \end{pmatrix}, \tag{6}$$

where we have replaced a' by a, b' by b and so on. Comparing this effective Hamiltonian with the original one in equation (1) for $\Delta_0 = 0$, it is seen that the nonlinear parameter c_Z can be regarded as a re-scaled parameter c, and the new nonlinear terms containing c_Y arise as a surprise. In addition, the ratio of the two nonlinear parameters c_Z and c_Y is given by $[1 + J_0(2\Delta_0/\omega)]/[1 - J_0(2\Delta_0/\omega)]$, which is easily adjustable by tuning the ratio Δ_0/ω.

In terms of the mean-field eigen-energies of H_{eff} as a function γ, three typical level structures of H_{eff} are depicted in figure 1. The structures represented by the solid lines in

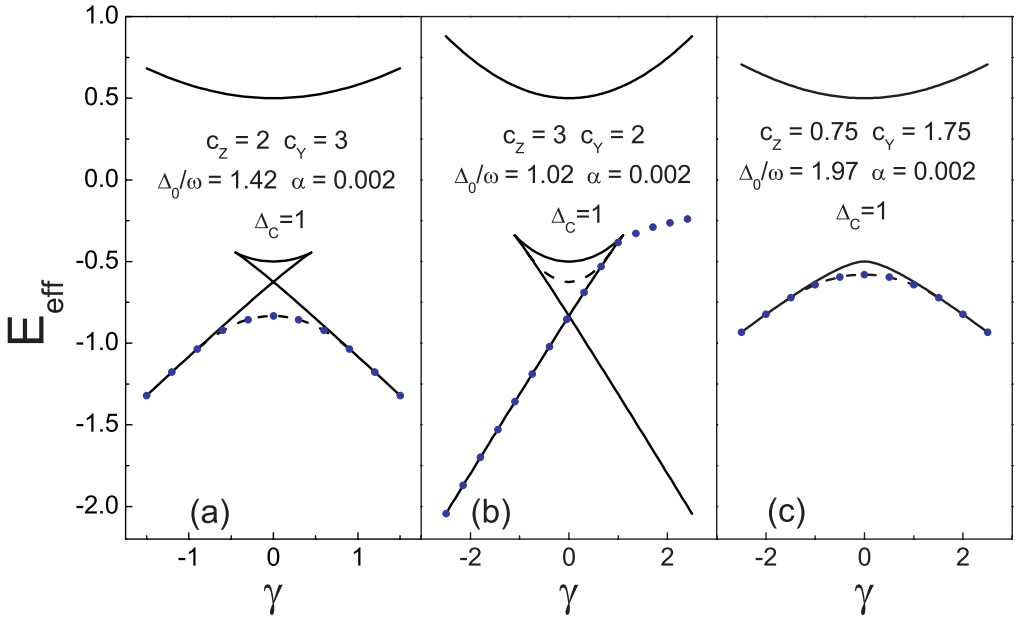

Figure 1. Eigen-energy structures of the effective Hamiltonian in equation (6) that describes NLZ processes in a high-frenquency and large-amplitude driving field. The effective Hamiltonian is obtained with a high-frequency approximation. The discrete points represent the time-evolving expectation value of the mean-field energy when γ increases in one adiabatic process. Along with other parameters, the values of the nonlinear parameter c and the driving frequency ω are indicated in the three panels. As mentioned in the text, all variables are appropriately scaled and hence dimensionless.

figure 1 are also typical in non-driven NLZ models [14], but the dashed lines (each of them is associated with double-degenerate eigenstates) in figure 1 are entirely induced by the high-frequency driving field. For an NLZ process with γ increasing at a very small rate of $\alpha = 0.002$ (hence an adiabatic NLZ process), the time-evolving expectation values of the mean-field energy associated with $H_{\rm eff}$ are shown by the discrete points in figure 1. Clearly, for the two cases in figures 1(a) and (c), the evolution of the system perfectly follows the new eigenstates (dashed lines). The driving field can hence dramatically affect the dynamics of adiabatic following. Indeed, in the case of figure 1(a), if there were no additional levels induced by the driving field, then the loop structure there will necessarily cause the adiabatic following to break down (this is analogous to what is observed in non-driven NLZ models [14] and will be also seen below). For other important findings in this high-frequency large-amplitude regime, please see [16].

The high-frequency approximation used here is also applicable to high-frequency and small-amplitude fields. However, if $\Delta_0/\omega \ll 1$, then $J_0(2\Delta_0/\omega) \sim 1$, $c_Z \sim c$, $c_Y \sim 0$ and the effective Hamiltonian in equation (6) will essentially reduce to the Hamitonian of equation (1) with $\Delta_0 = 0$. That is, in cases of $\Delta_0/\omega \ll 1$, the present high-frequency approximation based on the (a', b') representation does not directly give useful insights into the dynamics. Fortunately, in these cases the RWA treatment becomes valid and more advantageous to use. This is discussed in detail in the next section.

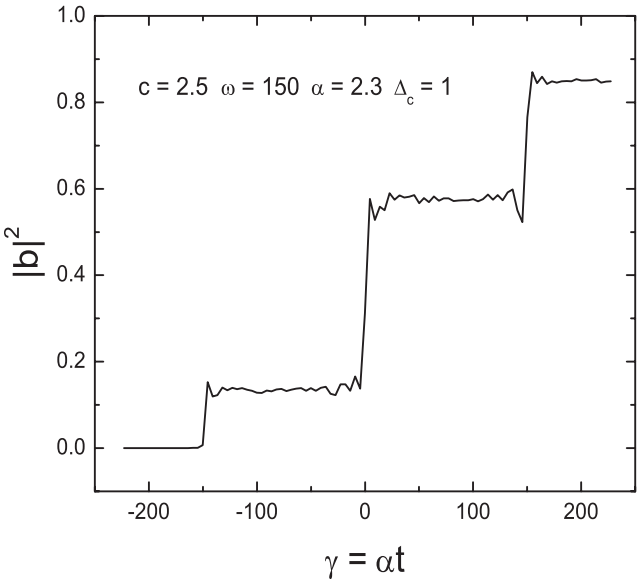

Figure 2. Transition probability $|b(t)|^2$ as a function of αt, with the phase parameter $\beta = 0$. The driving field is in the RWA regime. Three well-separated NLZ transitions can be seen here.

4. High-frequency and small-amplitude driving field

4.1. RWA

In the high-frequency and small-amplitude regime, we adopt the RWA for understanding the effects of a driving field on NLZ processes. The off-diagonal coupling term in equation (1) is now understood as a superposition of three terms,

$$\Delta = \frac{\Delta_0}{2}\left[\exp(-\mathrm{i}\omega t - \mathrm{i}\beta) + \exp(\mathrm{i}\omega t + \mathrm{i}\beta)\right] + \Delta_{\mathrm{C}}, \tag{7}$$

where the first two terms represent the circular modulation with frequency ω and $-\omega$, and the last constant term can be regarded as a circular modulation with zero frequency. Consistent with the high-frequency assumption, the effects of the three circular modulation terms can be analyzed separately. To illustrate this, we depict in figure 2 a typical numerical result for this parameter regime. Evidently, the transitions primarily occur in three small time windows around $\gamma \sim -\omega, 0, \omega$, each of them is associated with one of the three circular modulation terms in equation (7).

For the sake of a direct comparison between driven NLZ processes and the driven LZ processes studied in [11], we set $\Delta_{\mathrm{C}} = 0$ in the following. We then only need to consider two circular modulation terms. The effects of the first circular modulation term $\frac{\Delta_0}{2}\exp(-\mathrm{i}\omega t - \mathrm{i}\beta)$ become obvious in a rotating frame. We hence introduce another pair of wave-function parameters $(\tilde{a}, \tilde{b})$.

$$\begin{aligned} \tilde{a} &= a \exp\left[-\tfrac{1}{2}\mathrm{i}(\omega t + \beta)\right], \\ \tilde{b} &= b \exp\left[\tfrac{1}{2}\mathrm{i}(\omega t + \beta)\right]. \end{aligned} \tag{8}$$

Using this representation and neglecting the counter-rotating terms, one obtains

$$\mathrm{i}\frac{\partial}{\partial t}\begin{pmatrix}\tilde{a}\\ \tilde{b}\end{pmatrix} = \tilde{H}_{+}(t)\begin{pmatrix}\tilde{a}\\ \tilde{b}\end{pmatrix}, \tag{9}$$

where the RWA effective Hamiltonian $\tilde{H}_{+}(t)$ is given by

$$\tilde{H}_{+}(t) = \frac{1}{2}\begin{pmatrix}\gamma_{+} + c(|\tilde{b}|^2 - |\tilde{a}|^2) & \frac{\Delta_0}{2}\\ \frac{\Delta_0}{2} & -\gamma_{+} - c(|\tilde{b}|^2 - |\tilde{a}|^2)\end{pmatrix}, \tag{10}$$

with $\gamma_{+} = \gamma + \omega$. This Hamiltonian is essentially identical to that for a non-driven NLZ model, with the bias parameter γ shifted by ω and with the effective static coupling term determined by the amplitude of the periodic driving field. This explains the observation from figure 2 that one main transition window is roughly at $\gamma \sim -\omega$. Because $|b|^2 = |\tilde{b}|^2$, this RWA treatment also indicates that for a fixed initial state, the quantum population at the end of such a transition window should not depend on β. Similar treatments apply to the other circulation modulation term $\frac{\Delta_0}{2}\exp(\mathrm{i}\omega t + \mathrm{i}\beta)$, yielding the following effective Hamiltonian

$$\tilde{H}_{-}(t) = \frac{1}{2}\begin{pmatrix}\gamma_{-} + c(|\tilde{b}'|^2 - |\tilde{a}'|^2) & \frac{\Delta_0}{2}\\ \frac{\Delta_0}{2} & -\gamma_{-} - c(|\tilde{b}'|^2 - |\tilde{a}'|^2)\end{pmatrix}, \tag{11}$$

with $\tilde{a}' = a\exp[\frac{1}{2}\mathrm{i}(\omega t + \beta)]$ and $\tilde{b}' = b\exp[-\frac{1}{2}\mathrm{i}(\omega t + \beta)]$. Here, the effective bias is $\gamma_{-} = \gamma - \omega$, and as a result the main transition window will be close to $\gamma \sim \omega$.

Because the RWA treatment here is seen to be independent of the nonlinear parameter c, it applies as well to those driven (linear) LZ processes considered in [11]. Hence, for either NLZ or LZ processes, a periodic driving field is expected to shift the main quantum transition window at $\gamma \sim 0$ to two new windows close to $\gamma \sim \mp\omega$ (how the exact locations of the transition windows depend on c will be discussed later).

4.2. Phase-dependence weakened by strong nonlinearity

The above RWA treatment makes it clear that the NLZ dynamics in this regime can be described by effective Hamiltonians analogous to that for non-driven cases. However, because the final state of the transition window around $\gamma \sim -\omega$ becomes the initial state of the second transition window around $\gamma \sim \omega$, the driven dynamics should be much richer than in non-driven cases. Indeed, in the linear case with $c = 0$, the analytical result from [11] predicts that the final transition probability is given by

$$|b(\infty)|^2 = 4\exp(-\pi\,\Delta_0^2/8\alpha)\left[1 - \exp(-\pi\,\Delta_0^2/8\alpha)\right]\cos^2\beta, \tag{12}$$

where β is the phase of the driving field defined hereinbefore. Because the transition probability of the first LZ sub-process does not depend upon β, the factor $\cos^2(\beta)$ in equation (12) reflects how the net result associated with the second transition window is affected by the first one. Alternatively, this $\cos^2(\beta)$ factor can be interpreted as a quantum interference between two LZ sub-processes at two time windows [11]. This intriguing phase-dependence might be useful in determining an unknown value of β [11].

How does the nonlinear self-interaction of a BEC affect this $\cos^2(\beta)$-dependence of the final transition probability? Unable to obtain an analytical solution, we choose to examine this issue computationally. Typical results for a rather rapid ramping of γ are shown in figure 3.

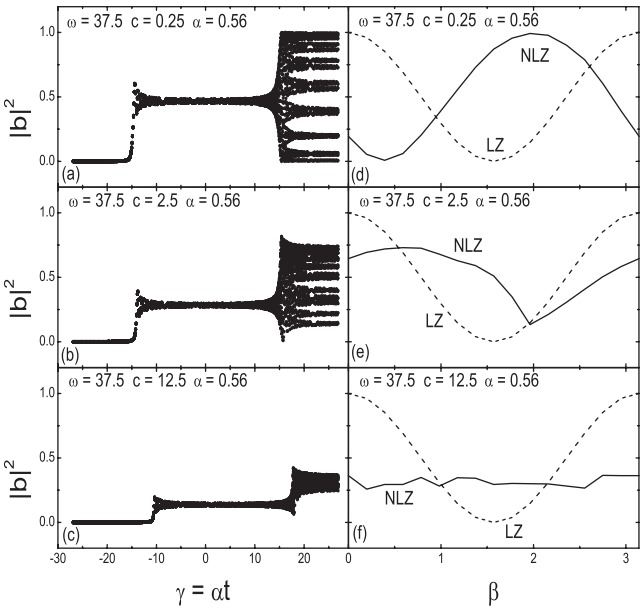

Figure 3. Left panel: transition probability $|b|^2$ as a function of αt, with $\alpha = 0.56$, $\omega = 37.5$ and different values of the nonlinear parameter c and the phase parameter β. Right panel: final NLZ transition probability $|b(\infty)|^2$ (solid lines) as a function of β. Dashed lines represent the theoretical linear result of equation (12) that displays a $\cos^2(\beta)$ dependence.

The ramping rate is chosen to be $\alpha = 0.56$ such that the linear result of equation (12) yields the maximal transition probability. Panels (a), (b) and (c) of figure 3 depict the time-evolving occupation probability $|b|^2$ as a function of αt, with the initial conditions $a = 1$ and $b = 0$. In each of the three panels, results for a number of β values are plotted collectively. For all the shown cases two main quantum transition windows can be clearly seen, consistent with our expectation based on the RWA analysis. Comparing figures 3(a) and (b) with figure 3(c), it is seen that as the nonlinear strength c increases, the final transition probabilities for different values of β tend to converge to a common value, i.e. they become less and less sensitive to β. To be more quantitative, we extract the β-dependence from figures 3(a)–(c) and then compare it (right panels in figure 3) with the linear result of equation (12). For the case of $c = 0.25$ (right upper panel of figure 3), the β-dependence of the final transition probability $|b(\infty)|^2$ exhibits a remarkable phase shift as compared with the linear result (dashed line). This phase-shift effect might be useful in determining a small but unknown value of c. For cases with sufficiently strong self-interaction (right bottom panel of figure 3), $|b(\infty)|^2$ changes little as β varies, constituting a sharp contrast to the $\cos^2(\beta)$ dependence in linear cases.

The weakened β-dependence due to strong nonlinearity requires a qualitative explanation. Consider the state after the first transition window, i.e. the initial state for the second NLZ sub-process. As β varies, the occupation populations associated with this intermediate state can be hardly changed (as is evident from the above RWA treatment), but the relative phase between the amplitudes $\tilde{a}'$ and $\tilde{b}'$ will be affected. With this understanding, we explain below the observed weakened β-dependence of $|b(\infty)|^2$ in terms of the increasing insensitivity of the second NLZ sub-process on the quantum phase of its initial state.

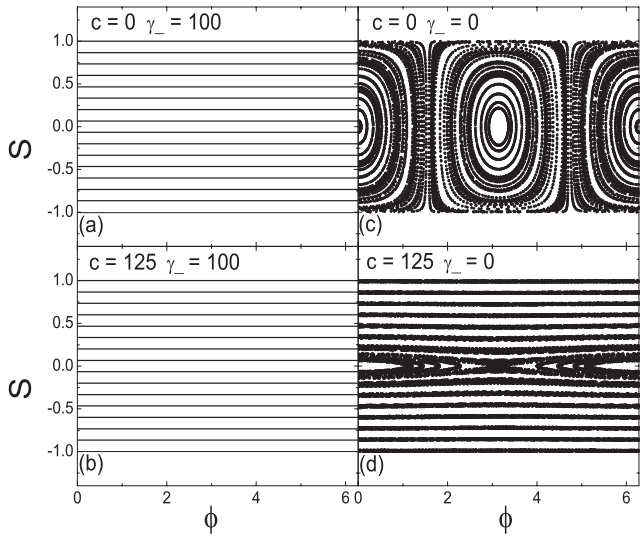

Figure 4. Phase-space structure associated with the mapped classical Hamtonian in equation (13), in terms of the dimensionless variables S and ϕ defined in the text. For large c, most phase-space invariant curves will be, independent of the value of $\gamma_- = \gamma - \omega$, almost straight lines perpendicular to the S-axis.

Let us map exactly the mean-field dynamics of the effective Hamiltonian in equation (11) to that of a classical Hamiltonian system, with the canonical variables $S = |\tilde{b}'|^2 - |\tilde{a}'|^2$ and ϕ [13, 16, 18], with ϕ the relative phase between the amplitudes $\tilde{a}'$ and $\tilde{b}'$. The mapped classical Hamiltonian, denoted by $\tilde{H}_c$, is then given by [13]

$$\tilde{H}_c = \frac{1}{2}\left[-\gamma_- S - \frac{c}{2}S^2 + \frac{\Delta_0}{2}\sqrt{1-S^2}\cos\phi\right]. \tag{13}$$

With this mapping, the phase of the initial state for the second NLZ sub-process apparently becomes the initial value of the coordinate ϕ. Further, the final transition probability $|b(\infty)|^2$ is given by $[S(\infty)+1]/2$.

Figure 4 compares the phase-space structure of $\tilde{H}_c$ for $\gamma_- = \gamma - \omega = 0$ and that for $\gamma_- = 100$. Consider first the upper two panels for $c = 0$. In the regime of large γ_- (figure 4(a)), the phase-space curves become straight lines perpendicular to the S-axis, with their S values determining $|b(\infty)|^2$. In the regime around $\gamma_- = 0$ (figure 4(c)), the phase-space invariant curves rotate around elliptic fixed points, with their oscillation amplitude in S sensitively dependent upon ϕ. Clearly then, if γ_- is scanned rather rapidly, the range of S values for $\gamma_- = 0$, which depends on the initial value of ϕ, will determine the range of S and hence the possible values of $|b(\infty)|^2$. This qualitatively explains the sensitive β-dependence in the linear case. By contrast, as shown in figures 4(b) and (d), the phase-space structure for large c is largely independent of γ_-, with most of the phase-space curves being parallel lines perpendicular to the S-axis. The sensitive dependence of $S(\infty)$ on ϕ, and hence the sensitive dependence of $|b(\infty)^2|$ on β, must be weakened for large c. Indeed, in the large c limit, one may only keep the $-cS^2/2$ term of $\tilde{H}_c$. $\tilde{H}_c$ then becomes the Hamiltonian for a 'free-particle' system, with a trivial phase-space structure filled with straight lines perpendicular to the S-axis. As such, the β-dependence of $|b(\infty)^2|$ in the large c limit will disappear altogether. This completes our qualitative explanation of the weakened β-dependence due to increasing nonlinearity.

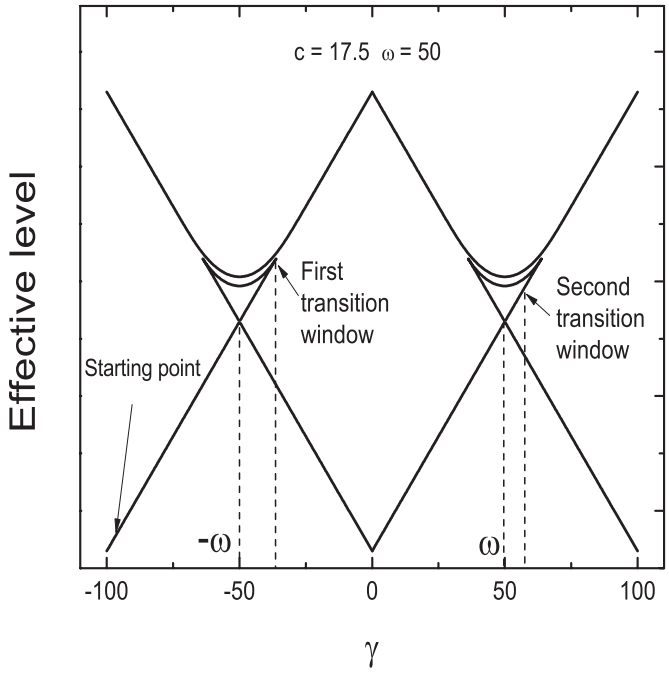

Figure 5. Schematic energy level structures of the RWA static Hamiltonians $\tilde{H}_+$ in equation (10) and $\tilde{H}_-$ in equation (11). $c = 17.5$ and $\omega = 50$. All variables are appropriately scaled and hence dimensionless.

Finally, we discuss another interesting observation made from figure 3. Comparing figures 3(a)–(c), one notes that the first transition window is delayed more and more as the nonlinear strength c increases. The delay of the second transition window as a function of c is however less apparent. To rationalize this observation, we first note that in the cases with negligible c, the standard picture based on linear LZ processes applies and the two transition windows should be centered precisely at $\gamma \sim -\omega$ and $\gamma \sim +\omega$. In the cases with large c, the effective Hamiltonians $\tilde{H}_+$ and $\tilde{H}_-$ obtained in our RWA treatment are expected to display loop structures, in the same manner as in non-driven NLZ models [14]. One typical example with $c = 17.5$ and $\omega = 50$ is shown in figure 5, where both $\tilde{H}_+$ and $\tilde{H}_-$ display a loop structure in the lower branch of the energy levels. Due to the loop structure of $\tilde{H}_+$, the increase in γ from a very negative value will not cause any significant transition to the upper branch at $\gamma \sim -\omega$. Rather, significant population transfer occurs only until the system reaches the right 'edge' of the loop, thus postponing the first transition window. In addition, because the loop structure is bigger for larger c, the first transition window will be postponed more as c increases.

Interestingly, after the first NLZ sub-process, the system will in general occupy both the upper and lower levels considerably. Then, as γ continues to increase in the positive regime, those populations on the upper branch will make significant transitions at $\gamma \sim \omega$, whereas those on the lower branch will delay their transitions again. The overall result is that the precise location of the second transition window becomes less definitive and more dependent on the details of the dynamics. With this recognition, we schematically place the second transition window in figure 5 between $\gamma \sim \omega$ and the right edge of the right loop structure.

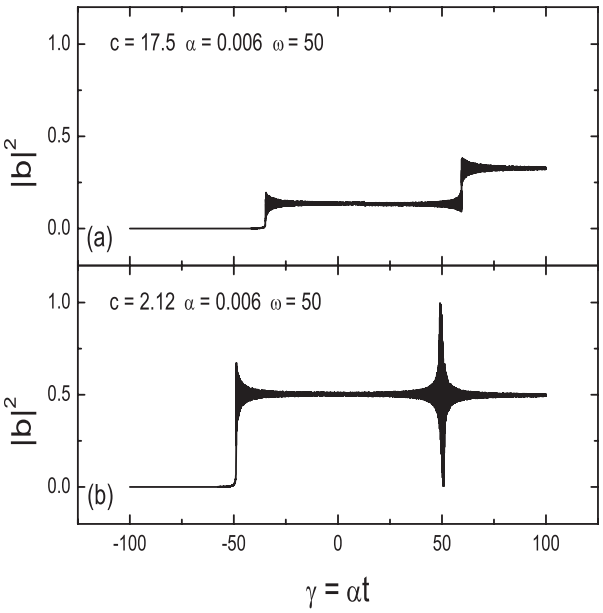

Figure 6. Transition probability $|b(t)|^2$ as a function of αt, for a small value of $\alpha = 0.006$ that simulates the dynamics in the adiabatic limit. Panels (a) and (b) are for two different values of c. In each case the results for a number of β values are plotted collectively. The large final values of $|b|^2$ are induced entirely by the nonlinear nature of the system.

4.3. Nonlinearity-induced transition probabilities

Equation (12) contains another intriguing and stimulating result for driven linear LZ processes. That is, in the adiabatic limit $\alpha \to 0$, the final transition probability $|b(\infty)|^2$ becomes zero for any β. The associated physical picture is as follows: after the first transition window of a linear driven LZ process, the adiabatic population transfer is already complete. But then the system approaches the second transition window, which transfers all the population back to the initial mode. In other words, for linear driven LZ processes, the transitions associated with the two time windows $\gamma \sim \mp\omega$ exactly cancel each other in the adiabatic limit. Such a strong result for linear systems motivates us to examine the driven NLZ processes in the same adiabatic limit.

For two values of the nonlinear parameter c, figure 6 shows the time-evolving occupation probability $|b|^2$, using a sufficiently small value of α for simulating the dynamics in the adiabatic limit. In each case, results with different values of β are plotted collectively. In all these cases, it is seen that the quantum transition probabilities at the end of the first transition window are far from unity. Because in linear cases the adiabatic population transfer after the first transition window should be always unity, the incomplete population transfer shown in figure 6 after the first transition window constitutes direct evidence of considerable NLZ tunneling in the adiabatic limit. Analogous NLZ tunneling in the second time window can also be expected. As to the final transition probability $|b(\infty)|^2$ (final values of $|b|^2$), they are seen to be insensitive to β. This phase insensitivity is similar to previous non-adiabatic cases with considerable c values. But more noteworthy is, $|b(\infty)|^2$ is $\sim$0.35 for $c = 17.5$ in figure 6(a) and as large as $\sim$0.5 for $c = 2.12$ in figure 6(b). Considering that $|b(\infty)|^2$ should be precisely zero if $c = 0$, the large transition probabilities $|b(\infty)|^2$ here are induced entirely by the nonlinear nature of the system.

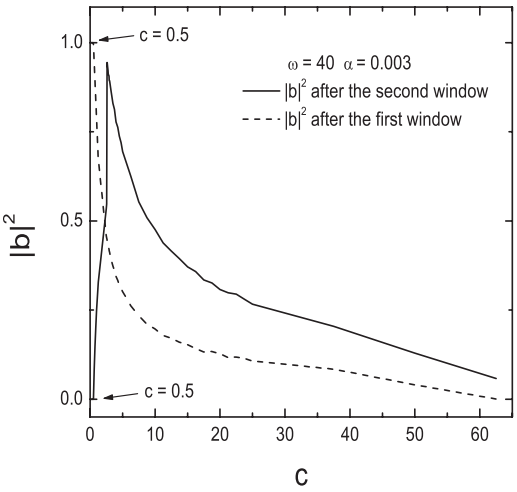

Figure 7. The final transition probability $|b(\infty)|^2$ (solid line) as a function of the nonlinear strength c, for a high-frequency and small-amplitude driving field. The dashed line shows the transition probability right after the first transition window.

In addition, comparing figures 6(a) and (b), one also sees that the larger c is, the more delayed the first transition window will be. This observation is analogous to what is found in figure 3.

To further motivate interests in the nonlinearity-induced transition probabilities in driven NLZ processes, we calculate $|b(\infty)|^2$ in many adiabatic cases that cover a wide range of c values. A typical result, obtained with $\omega = 40$ and $\alpha = 0.003$, is depicted in figure 7. The non-monotonic dependence of $|b(\infty)|^2$ upon c is apparent. In particular, for any $c < 0.5$, the transition probability right after the first transition window is close to unity and becomes essentially zero after the second transition window. This behavior is the same as in linear driven LZ processes in the adiabatic limit. Hence, for the RWA regime studied here, the threshold value for observing nonlinearity-induced population transfer at the end of the adiabatic process is around $c \sim 0.5$. Figure 7 also indicates that for very large values of c, $|b(\infty)|^2$ decays back to zero again. For intermediate values of c, the final transition probability can be significant. Indeed, the peak value of $|b(\infty)|^2$ as a function of c is found to be as large as $\sim$0.95.

Note that the c value here is scaled by Δ_0, it is clear that by tuning the amplitude of the driving field one may realize the peak value of $|b(\infty)|^2$ observed in figure 7, without actually tuning the natural scattering length or the number of bosons of the BEC. Hence, a nearly complete population inversion is made possible by a periodic driving field in the RWA regime. This finding offers a potentially useful scenario for improving the adiabatic population transfer in NLZ processes. Interestingly, in the high-frequency and large-amplitude regime discussed in section 3, the adiabatic population transfer is improved by suppressing the NLZ tunneling; whereas, the nearly complete population transfer here is based on the overall effect of two NLZ tunneling processes.

Combining (i) the shifted β-dependence of $|b(\infty)|^2$ for small c, (ii) the weakened β-dependence of $|b(\infty)|^2$ for large c, (iii) the delay of the first transition window as a function of c and (iv) the nonlinearity-induced transition probabilities in the adiabatic limit, one may also design strict tests to check the validity of a two-mode description of a driven many-body quantum system.

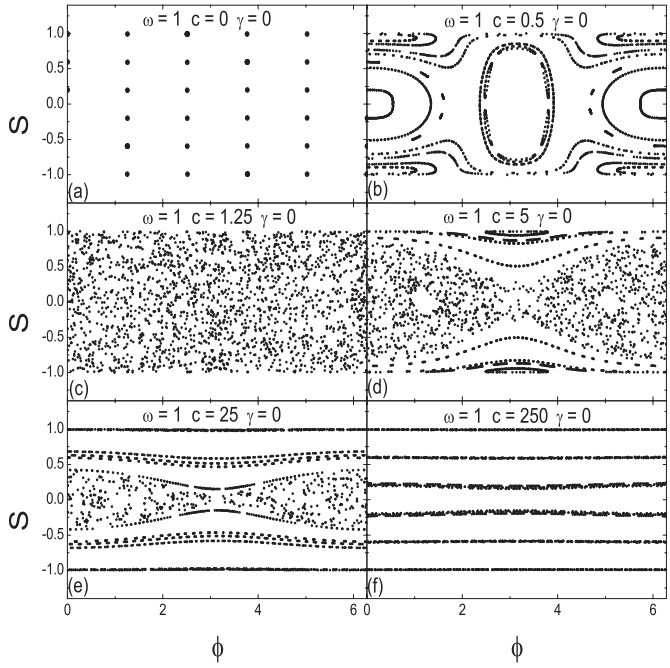

Figure 8. Phase-space structure associated with the classical effective Hamiltonian in equation (14) with $\beta = 0$, in terms of s and ϕ defined in the text, for various values of c. The driving frequency is given by $\omega = 1$. As mentioned in the text, all variables are appropriately scaled and hence dimensionless.

5. Low-frequency driving fields

If the driving frequency ω is comparable to, or smaller than, c and Δ_0, we call it a low-frequency case. In this regime the previous high-frequency approximation or RWA does not apply. As it turns out, complications arise here due to the emergence of Hamiltonian chaos on the mean-field level.

Using the same approach in section 4.2, let us first map the driven NLZ dynamics described by equation (1) (with $\Delta_C = 0$) to that of a classical Hamiltonian,

$$H_c(t) = \frac{1}{2}\left[-\gamma S - \frac{c}{2}S^2 + \Delta_0 \cos(\omega t + \beta)\sqrt{1 - S^2}\cos\phi\right], \tag{14}$$

where S is given by $(2|b|^2 - 1)$ and ϕ is now the relative phase between the amplitudes a and b. Because ω is small, it is impossible to divide the driven NLZ process into two sub-processes. But this also implies that, roughly speaking, the phase-space structure at $\gamma \sim 0$ will be most important in understanding the mean-field dynamics. As such, we show in figure 8 the typical behavior of the Poincaré surface of section of $H_c(t)$ with $\gamma = 0$, $\omega = 1$, $\beta = 0$ and with the nonlinearity parameter c ranging from 0 to 250. It is seen that for intermediate values of c, the phase-space is completely chaotic, whereas for small or large values of c, the dynamics is primarily regular.

In figure 9, we plot $|b(\infty)|^2$ as a function of β, with the values of ω same as in figure 8. Consider first figure 9(a) for the $c = 0$ case. The β-dependence is seen to be rather weak, in contrast to the $\cos^2(\beta)$ result in the RWA regime. In addition, $|b(\infty)|^2$ is small for the entire

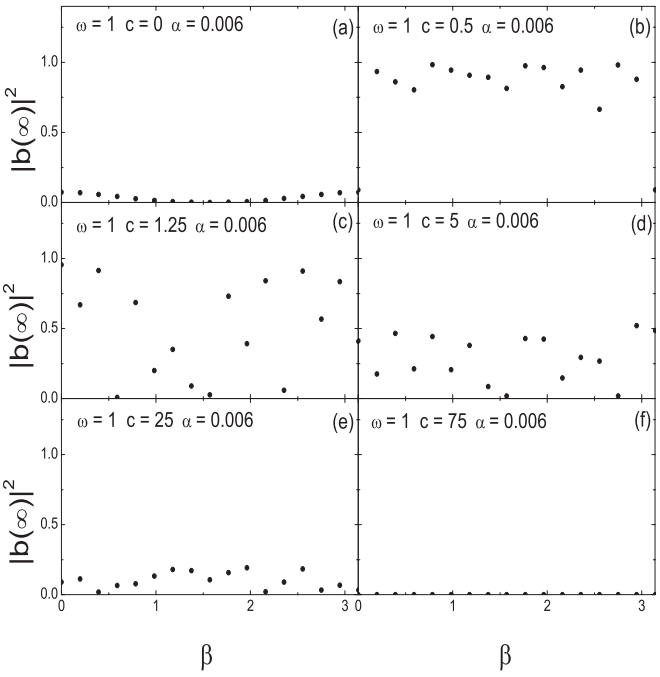

Figure 9. The final probability $|b(\infty)|^2$ as a function of phase β for $\alpha = 0.006$ and $\omega = 1$. Results here should be connected with those in figure 8.

range of β. Next, in figure 9(b) for $c = 0.5$, the β-dependence remains weak, but the final transition probability $|b(\infty)|^2$ becomes very significant in general: it can even reach almost 100% for certain values of β. We hence observe nonlinearity-enhanced population transfer again, but now outside the RWA regime. As c is increased to $c = 1.25$ in figure 9(c), drastic and full-range oscillations of $|b(\infty)|^2$ are observed. Because figure 8(c) shows that this case corresponds to full Hamiltonian chaos, the full-range oscillation in figure 9(c) is clearly related to the underlying complete chaos on the mean-field level. As the nonlinearity parameter c further increases, the oscillation range of $|b(\infty)|^2$ decreases, consistent with the observation from figure 8 that the chaotic layer becomes smaller and smaller. In the case of $c = 75$ in figure 9(f), there is essentially no transition probability for any value of β. We have also done more detailed analysis of how mean-field trajectories should move as γ is ramped, confirming that the size of the chaotic layer determines the oscillation range of $|b(\infty)|^2$.

Comparing results in figures 9(c) and (d) with those in figures 9(a) and (b), one finds another interesting aspect of driven NLZ dynamics. That is, contrary to our observation in the RWA regime, nonlinearity may also enhance the β-dependence of $|b(\infty)|^2$. Note, however, that the strong β-dependence observed here is due to the mean-field chaos. Because chaos brings about strong instabilities and hence large fluctuations in the quantum system, results directly associated with the mean-field chaos should be applied with caution. For example, the validity of the mean-field treatment itself in the chaotic cases might be questionable when the number of particles in a BEC is not extremely large. This being so, a low-frequency driving field generating the mean-field chaos could be used to study effects of quantum fluctuations via the β-dependence of $|b(\infty)|^2$.

6. Conclusion

Nonlinear extensions of LZ processes, and in particular, NLZ processes in a periodic driving field, are of importance in realizing the control of interacting many-body systems. By considering different parameter regimes of a periodic driving field, we have exposed a number of interesting dynamical phenomena in driven NLZ processes. Many of these dynamical phenomena can be used for the control of NLZ processes by a driving field.

In the high-frequency and large-amplitude regime, a driving field can effectively generate new self-interaction terms that are absent in non-driven two-mode NLZ models. The field can hence induce new energy-level structures and can be useful in simulating new systems not considered before. A driving-field-based scenario for the suppression of undesired NLZ tunneling probabilities also becomes possible.

In the high-frequency and small-amplitude regime, driven NLZ processes are also much different from driven LZ processes in at least three aspects. Firstly, for small nonlinearity strength the final transition probability shows a shifted phase-dependence on the driving field. Secondly, for strong nonlinearity strength the transition probability shows a much weakened phase-dependence upon the driving field. Thirdly, in the adiabatic limit, significant transition probabilities become a purely nonlinear effect, because they were precisely zero in the absence of the self-interaction. These differences between driven NLZ and driven LZ processes suggest that a driving field may be used for directly exposing and measuring nonlinear effects. Furthermore, the adiabatic population transfer entirely based on the nonlinear nature of the system can be almost complete for certain amplitudes of the driving field, thus leading to an interesting approach to the improvement of adiabatic population transfer in the presence of NLZ tunneling.

In the third low-frequency regime, nonlinearity may also enhance the final transition probability as well as its dependence on the phase of the driving field. The enhanced phase-dependence occurs for intermediate nonlinear strength, where the NLZ dynamics displays Hamiltonian chaos. A driving field in this regime can therefore be used for studies of quantum fluctuations beyond the mean-field level, as well as studies of manifestations of mean-field chaos in the final transition probabilities.

To conclude, we have exposed many interesting aspects of driven NLZ processes, by considering different parameter regimes of a single-frequency and constant-amplitude driving field. It is plausible that the driven NLZ processes are even much richer in the presence of more complex driving fields, such as those with multiple frequency components that have time-evolving amplitudes and phases. It should also be interesting to extend our NLZ treatments to other many-body generalizations of LZ processes that can go beyond the mean-field level [29]–[31].

Acknowledgment

JG was supported by start-up funding (WBS grant numbers R-144-050-193-101 and R-144-050-193-133) and NUS ‘YIA’ funding (WBS grant number R-144-000-195-123), both provided by the National University of Singapore. PH acknowledges financial support from the Deutsche Forschungsgemeinschaft via the Collaborative Research Centre SFB-486, project A10, and from the German Excellence Cluster *Nanosystems Initiative Munich* (NIM).

References

[1] Landau L D 1932 *Phys. Z. Sowjetunion* **2** 46
Zener G 1932 *Proc. R. Soc. Lond.* A **137** 696
[2] Ankerhold J and Grabert H 2003 *Phys. Rev. Lett.* **91** 016803
[3] Ithier G, Collin E, Joyez P, Vion D, Esteve D, Ankerhold J and Grabert H 2005 *Phys. Rev. Lett.* **94** 057004
[4] Zagoskin A M, Ashhab S, Johansson J R and Nori F 2006 *Phys. Rev. Lett.* **97** 077001
[5] Wubs M, Kohler S and Hänggi P 2007 *Physica* E **40** 187
[6] Földi P, Benedict M G and Peeters F M 2008 *Phys. Rev.* A **77** 013406
[7] Saito K and Kayanuma Y 2004 *Phys. Rev.* B **70** 201304
[8] Miyashita S 1995 *J. Phys. Soc. Japan* **64** 3207
Wernsdorfer W and Sessoli R 1999 *Science* **284** 133
[9] Grifoni M and Hänggi P 1998 *Phys. Rep.* **304** 229
[10] Saito K, Wubs M, Kohler S, Kayanuma Y and Hänggi P 2007 *Phys. Rev.* B **75** 214308
[11] Wubs M, Saito K, Kohler S, Kayanuma Y and Hänggi P 2005 *New J. Phys.* **7** 218
[12] Holthaus M 2001 *Phys. Rev.* A **64** 011601
[13] Liu J, Fu L, Ou B, Chen S, Choi D, Wu B and Niu Q 2002 *Phys. Rev.* A **66** 023404
[14] Wu B and Niu Q 2000 *Phys. Rev.* A **61** 023402
[15] Witthaut D, Graefe E M and Korsch H J 2006 *Phys. Rev.* A **73** 063609
[16] Zhang Q, Hänggi P and Gong J B 2008 *Phys. Rev.* A **77** 053607
[17] Kayanuma Y and Saito K 2008 *Phys. Rev.* A **77** 010101
[18] Wang G F, Fu L B and Liu J 2006 *Phys. Rev.* A **73** 013619
[19] Grossmann F, Dittrich T, Jung P and Hänggi P 1991 *Phys. Rev. Lett.* **67** 516
[20] Della Valle G, Ornigotti M, Cianci E, Foglietti V, Laporta P and Longhi S 2007 *Phys. Rev. Lett.* **98** 263601
[21] Kierig E, Schnorrberger U, Schietinger A, Tomkovic J and Oberthaler M K 2008 *Phys. Rev. Lett.* **100** 190405
[22] Weiss C and Teichmann N 2008 *Phys. Rev. Lett.* **100** 140408
[23] Gati R and Oberthaler M K 2007 *J. Phys. B: At. Mol. Opt. Phys.* **40** R61
[24] Shin Y *et al* 2004 *Phys. Rev. Lett.* **92** 050405
[25] Albiez M, Gati R, Fölling J, Hunsmann S, Cristiani M and Oberthaler M 2005 *Phys. Rev. Lett.* **85** 010402
[26] Jona-Lasinio M *et al* 2003 *Phys. Rev. Lett.* **91** 230406
[27] Matthews M R *et al* 1999 *Phys. Rev. Lett.* **83** 3358
[28] Luo X, Xie Q and Wu B 2007 *Phys. Rev.* A **76** 051802
[29] Kayali M A and Sinitsyn N A 2003 *Phys. Rev.* A **67** 045603
[30] Dobrescu B E and Pokrovsky V L 2006 *Phys. Lett.* A **350** 154
[31] Altland A and Gurarie V 2008 *Phys. Rev. Lett.* **100** 063602